Science of the Total Environment 599–600 (2017) 355–363

Contents lists available at ScienceDirect

Science of the Total Environment

journal homepage: www.elsevier.com/locate/scitotenv

High abundance of protein-like fluorescence in the Amerasian Basin of Arctic Ocean: Potential implication of a fall phytoplankton bloom

Meilian Chen [a], Seung-Il Nam [b], Ji-Hoon Kim [c], Young-Joo Kwon [a], Sungwook Hong [a], Jinyoung Jung [d], Kyung-Hoon Shin [e], Jin Hur [a,*]

[a] Department of Environment & Energy, Sejong University, Seoul 143-747, South Korea
[b] Division of Polar Paleoenvironment, Korea Polar Research Institute, Incheon 21990, South Korea
[c] Petroleum and Marine Research Division, Korea Institute of Geoscience and Mineral Resources, 124 Gwahang-no, Yuseong-gu, Daejeon 34132, South Korea
[d] Arctic Research Centre, Korea Polar Research Institute, Incheon 21990, South Korea
[e] Department of Marine Sciences and Convergent Technology, Hanyang University, Ansan 15588, South Korea

HIGHLIGHTS

- Importance of CDOM dynamics in the fast-changing Arctic ecosystem is highlighted.
- Optical properties of DOM were spatially examined in the Arctic Ocean area.
- High levels of protein-like fluorescence were newly found in the region.
- All observed data including remote sensing data supported fall phytoplankton bloom.
- A lateral spreading of nutrients and DOM was suggested along shelf-slope-basin.

GRAPHICAL ABSTRACT

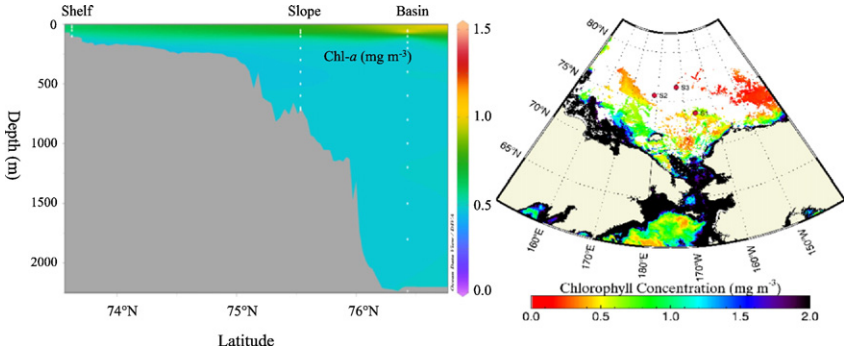

ARTICLE INFO

Article history:
Received 23 February 2017
Received in revised form 28 April 2017
Accepted 28 April 2017
Available online 4 May 2017

Editor: D. Barcelo

Keywords:
Dissolved organic matter
Excitation-emission matrix (EEM)
Fall phytoplankton bloom
Remote sensing
Arctic Ocean

ABSTRACT

The seawater samples from the Chukchi and East Siberian Seas were collected along a shelf-slope-basin gradient and analyzed for chromophoric and fluorescent DOM (i.e., CDOM and FDOM, respectively). Unexpected high protein-like FDOM (0.35 ± 0.40 and 0.24 ± 0.34 RU for peaks B and T, respectively) levels were identified, which corresponded to 1–2 orders of magnitude higher than those documented by previous reports. This unique phenomenon could be attributed to a fall phytoplankton bloom. The seawater chl-*a* data, estimated from in situ fluorescence measurements and satellite remote sensing data, showed the subsurface chl-*a* maximum of up to 1.52 mg m^{-3} at ~25–70 m depths and the surface monthly average values (August 2015) up to 0.55 to 0.71 mg m^{-3}, which fall in the range of ~0.5–2.0 mg m^{-3} during fall phytoplankton blooms in this area. Meanwhile, the depth profile of DOM parameters revealed subsurface maxima of protein-like fluorescence peaks along the shelf-slope gradient. The positive correlations between the protein-like peaks and biological index implied the lateral transport of DOM and nutrients from the shelf to the slope and basin. Despite still being a largely ice-covered environment, potential shifts in the ecosystem appear to make progress in response to changing climate in the Arctic Ocean.

© 2017 Elsevier B.V. All rights reserved.

* Corresponding author.
E-mail address: jinhur@sejong.ac.kr (J. Hur).

http://dx.doi.org/10.1016/j.scitotenv.2017.04.233
0048-9697/© 2017 Elsevier B.V. All rights reserved.

1. Introduction

The Arctic Ocean, which receives ~10% of global river discharges, occupies only <1% of the global ocean volume (Stein, 2008 and reference therein). It has a large drainage basin area of 9.5×10^6 km^2, which contains 1100–1500 Pg C soil organic carbon including a large stock of permafrost (Rachold et al., 2004; Hugelius et al., 2014). Currently, the fluvial input transports about 25–36 Tg C yr^{-1} of dissolved organic carbon (DOC) and 12 Tg C yr^{-1} of particulate organic carbon (POC) into the Arctic Ocean (Rachold et al., 2004; Raymond et al., 2007; Holmes et al., 2012). As such, it plays a pivotal role in regional and global carbon budget and cycle.

Ongoing climate change accelerates terrestrial organic matter inputs of modern plant litter leachates during the spring freshet as well as during winter base flow when aged and degraded materials prevail (Stedmon et al., 2011). Moreover, the Arctic perennial sea ice cover has been declining at a rate of 9% per decade (Comiso, 2002). Global warming has also advanced sea ice melting in spring and delayed sea ice formation in fall at the seasonal ice coverage area. Multiple previous studies have proved that the extent and the concentration of the sea ice were closely related to the Arctic phytoplankton biomass, in which phytoplankton production was usually high along retreating ice edges where nutrients can be replenished by wind- or storm-driven water column vertical overturn (Wang et al., 2005; Perrette et al., 2011). Increase in the intensity and frequency of storms can lead to more episodic vertical mixing events (Inoue et al., 2015; Nishino et al., 2015). Furthermore, Ardyna et al. (2014) have observed via remote sensing that recent retreat of Arctic Ocean sea ice has triggered a shift from single spring bloom to double blooms (both spring and fall, a typical pattern at temperate latitudes) in some regions, which has been supported by a recent in situ measurement evidence in the Chukchi Shelf (Uchimiya et al., 2016). Given the large stock of organic carbon in this area and the pace of the climate change, it is urgent to better understand the characteristics and dynamics of dissolved organic matter (DOM) in this area in an era of rapidly changing Arctic.

To date, previous reports on the DOM optical characteristics in this region have primarily focused on the Arctic rivers (Spencer et al., 2009; Walker et al., 2013; Cory et al., 2014; Mann et al., 2016). These studies generally found that terrestrial humic-like fluorescent DOM (FDOM) dominated the optical properties of DOM in the Arctic Rivers. In the Arctic Ocean, Guéguen et al. (2012, 2014, 2015) carried out a series of seawater chromophoric DOM (CDOM) and FDOM investigations in the Amerasian Basin and Canadian Arctic Archipelago areas. The main findings include the depth- and basin-dependent patterns of optical DOM properties and significant correlations of terrestrial humic-like FDOM components with apparent oxygen utilization (AOU).

The optical methods based on ultraviolet-visible spectroscopy (UV–Vis) and fluorescence excitation-emission matrix (EEM) have the advantages of fast, sensitive, and solvent-free with small sample volume needed. These techniques have been successfully applied to trace DOM dynamics in various ecosystems in previous studies (Coble et al., 1998; Spencer et al., 2009; Walker et al., 2009, 2013; Chen et al., 2010; Stedmon et al., 2011; Hur and Cho, 2012; Guéguen et al., 2012, 2014, 2015; Mann et al., 2016; Chen and Jaffé, 2016).

In this study, we aimed to examine the optical characteristics of the Arctic seawater DOM for a time period from the late August and early September in the Chukchi and East Siberian Seas in the Arctic Ocean. The Chukchi Sea, downstream of the nutrient-enriched Pacific-sourced water, is the only area of inflowing water to the Arctic Ocean. This area is relatively less investigated for DOM studies. Furthermore, the sampling time of this study fell into the fall season, which can capture the DOM characteristics derived from the potential fall phytoplankton bloom in the Arctic Ocean, as suggested by previous satellite remote sensing (Ardyna et al., 2014) as well as a recent in situ observation in Chukchi Shelf (Uchimiya et al., 2016). All these situations are of benefit in inferring the potential origins and environmental factors shaping the seawater DOM characteristic in the study area.

2. Materials and methods

2.1. Sites description

Sampling sites were located in the shallow Chukchi Shelf (site JPC-1a or site S1), East Siberia Continental Slope (site JPC-3 or site S3), and Chukchi Basin (site JPC-4 or site S4) of the Arctic Ocean (Fig. 1). The locations and the site descriptions are summarized in Table S1. The modern Chukchi Sea is a marginal sea with seasonal ice cover, and it has an expansive shallow continental shelf and an extremely high primary productivity (Sakshaug, 2004). This high productivity is driven by light availability during seasonal open water condition and enriched nutrients replenished by Bering Shelf Anadyr Water (BSAW) entraining through the Bering Strait. The Bering Sea Water (BSW) and the Alaskan Coastal Water (ACW) dominate the Chukchi Sea circulation (Grebmeier et al., 1988). The BSW is a mixture of nutrients-enriched BSAW and nutrients-poor ACW (Grebmeier et al., 1988). The East Siberia Sea receives riverine discharge from the Kolyma and Indigirka rivers. Two major current systems, namely the Beaufort Gyre and the Transpolar Drift, dominate surface water circulation in the Arctic Ocean. The Beaufort Gyre occupies most of the Amerasian Basin, in which our study sites are located, while the Transpolar Drift is dominant in the Eurasian Basin. A switching between cyclonic and anticyclonic Beaufort Gyre was also observed (Morison et al., 2012). The direction and strength of the currents, however, may be affected by the Arctic Oscillation and El Niño-Southern Oscillation, which could lead to large inter-annual variations (Thompson and Wallace, 1998; Liu et al., 2004). As sites S3 and S4 were partially sea ice-covered, only site S1 was ice-free at the time of sampling from August 30th to September 5th, 2015.

2.2. Sampling

The samples were collected between late August to early September 2015 during the ARA06C Expedition. Both seawater and sediment pore waters were collected and the data on pore water study has been reported in a separate paper (Chen et al., 2016). The daily sea ice map and the concentration in the Arctic can be found elsewhere (www.meereisportal.de). Seawater sampling was carried out using a CTD/rosette system holding 24-10L Niskin bottles (SeaBird Electronics, SBE 911 plus) aboard the Korean icebreaker R/V *Araon* during the ARA06C cruise. For partially sea ice-covered sites S3 and S4, we tried to find non-ice covering area to get seawaters or broke the thin sea ice by the ice breaker. The in situ fluorescence data (Ex/Em: 470 nm/695 nm) was monitored while sampling for chl-*a* estimation. The seawaters were sampled with acid-cleaned syringes and filtered with a pre-cleaned in-line 0.20 μm disposable polytetrafluoroethylene filter (Advantec). The seawater aliquots were transferred into acid-cleaned Nalgene® high density polyethylene bottles for onboard, DOM, and nutrients analyses. The samples for DOM analyses were immediately stored in a freezer to avoid potential biodegradation on the long journey from Arctic back to land-based lab. It is noteworthy that freezing/thawing samples may have potential effects on DOM fluorescence signals due to susceptibility of humic-like fraction removal from solution (Thieme et al., 2016). Stedmon and Markager (2001) recommended to sterile filter samples through 0.2 μ m filters followed by storage in cool and dark in the fridge to keep DOM samples for spectroscopic analysis, which can made them stable for time period of several weeks. However, when longer storage time ranges are needed (such as on a scale of months, especially when sampling from polar regions), freezing has been a common practice for marine sample preservation (Walker et al., 2009; Stedmon et al., 2011; Logvinova et al., 2015). As such, same or similar sample storage methods are needed to facilitate ease of comparison. The samples for onboard analyses (chl-*a* fluorescence and

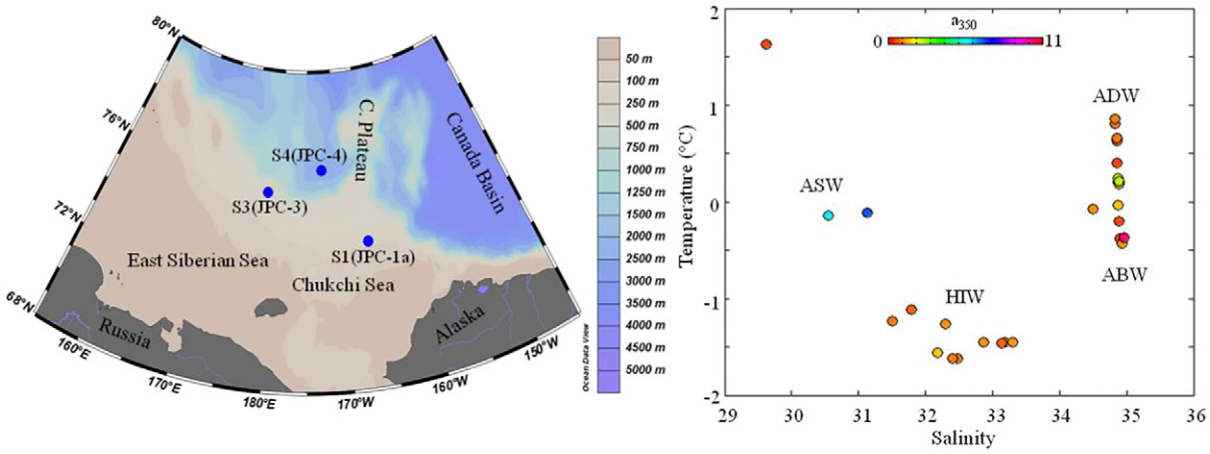

Fig. 1. Sampling sites in the Chukchi – East Siberian Seas of the Arctic (left) and T–S diagram for all the samples (right). ASW: Arctic Surface Water; HIW: Halocline Intermediate Water (50–200 m); ADW: Atlantic Deep Water; ABW: Arctic Bottom Water (>900 m). Map produced with Ocean Data View (Schlitzer, 2016).

oceanographic data) and nutrients measurements were stored in refrigerator (~4 °C).

2.3. Analytical measurements and data processing

The phosphate (PO_4^{3-}) and ammonium (NH_4^+) were measured using colorimetric methods with a spectrophotometer (Shimadzu UV-2450) at 885 nm and 640 nm, respectively (Gieskes et al., 1991). Salinity was determined by a reflectometer, and alkalinity was analyzed by titration using 0.1 N HCl onboard. The reproducibility of alkalinity was <2% based on the repeated analyses of the IAPSO (i.e., International Association for the Physical Sciences of the Oceans) standard seawater. The in situ fluorescence was measured with a chlorophyll fluorometer (model FLRTD, WET labs) with excitation channel centered at 470 nm and emission set to 695 nm. The chl-*a* sensor was calibrated prior to measurements. The signal is reported with 0–5 V DC analog output values with offset correction. The chl-*a* was calculated from the linear relationship between the fluorescence data measured in situ and the spectrophotometrically measured concentrations of chl-*a* (i.e., [chl-*a*] = 0.303 × $\text{fluorescence}_{470/695\text{nm}}$ + 0.496). We need to emphasize that caution must be taken when using this approach due to high variability of chl-*a* fluorescence quantum yield variability stemmed from photoacclimation and other physiological factors in various ecosystems (Cullen, 1982). Surface chl-*a* at ice-free site S1 was also retrieved using satellite remote sensing data by both MODIS (Moderate Resolution Imaging Spectroradiometer)-Aqua (EOS PM-1) and MODIS-Terra (EOS AM-1) (http://oceandata.sci.gsfc.nasa.gov, see supporting information for detailed procedures and satellite image). Due to sea ice and clouds conditions, only chl-*a* data at the ice-free site S1 in August 2015 was retrieved. Details regarding the measurements of other nutrients are described elsewhere (Kim et al., 2013; KIGAM, 2015). EEMs were obtained using a Hitachi F-7000 luminescence spectrometer (Hitachi Inc., Japan) at the excitation/emission (Ex/Em) wavelengths of 250–500/280–550 nm. The excitation and the emission scans were set at 5 nm and 1 nm steps, respectively, at a rate of 12,000 nm/min. Both the excitation and emission slits were 10 nm. Absorption spectra were scanned from 240 to 800 nm on a Shimadzu 1800 ultraviolet-visible (UV–Vis) spectrophotometer (Shimadzu Inc., Japan). All samples were transferred into a special capped cuvette in a nitrogen-filled glove box for the UV–Vis and EEMs measurements.

The procedures of post-acquisition corrections are available in a previous report (Chen et al., 2010). The procedures for Raman Unit (RU) normalization can be found elsewhere (Lawaetz and Stedmon, 2009). We utilized peak-picking instead of parallel factor analysis (PARAFAC) modeling due to the extremely high protein-like as compared to the humic-like moieties to avoid the exclusion of the humic-like components by the PARAFAC modeling. The Ex/Em wavelengths used for five protein-like and humic-like peaks were 280/310 (B), 280/340 (T), 315/400 (M), 260/420 (A), and 350/450 (C) according to the literature (Coble et al., 1998). The optical indices of biological index (BIX), fluorescence index (FI), humification index (HIX), slope ratio (S_R), and specific absorption coefficient $a^*_{CDOM}(254)$ were also calculated according to previous literature (Huguet et al., 2009; Parlanti et al., 2000; McKnight et al., 2001; Zsolnay et al., 1999; Weishaar et al., 2003; Helms et al., 2008).

3. Results

3.1. Water mass properties

Four water masses, namely Arctic Surface Water (ASW), Halocline Intermediate Water (HIW), Atlantic Deep Water (ADW), and Arctic Bottom Water (ABW), were identified in the study area according to the data of salinity, temperature, and ammonium (Fig. 1). The water masses maintain a stable stratification of the Arctic seawater due to a large riverine freshwater discharge, sea ice melting, and meteoric water (Cauwet and Sidorov, 1996). Stratification is weaker in the Chukchi Sea than those areas subject to more influence of river waters (Aagaard and Carmack, 1989). The ASW is a mixed layer of low-salinity and low temperature usually <50 m in depth, underlain by a complex HIW (50–200 m), followed by a warm and saline ADW and a layer of ABW (>900 m) (Fig. S1, Stein, 2008; Anderson and Amon, 2014). The water residence times (WRTs) for seawaters are variable depending on the layers. In general, relatively shorter (1 to10 yrs) WRTs were found for the ASW and HIW, while longer WRTs (25 to 30 yrs) were reported for the ADW and up to about 300 yrs for the ABW (Stein, 2008).

3.2. Variations of bulk DOM and the optical signatures along a shelf-slope-basin gradient

Our results were compared with those of the previous studies on the Arctic Ocean (Table 1). The CDOM values expressed using absorption coefficients (3.9 ± 3.4 m^{-1} at 254 nm and 1.6 ± 2.2 m^{-1} at 350 nm) were, however, generally comparable to those reported previously (Table 1). Meanwhile, the high absorption coefficient of CDOM at 254 nm observed in a previous study could not be comparable to this study since the East Siberian Shelf area is heavily affected by the high terrestrial inputs of the Siberian Rivers (Pugach et al., 2015). No significant differences of CDOM among the three sites were found in this study (Table S1).

The aromaticity index, or $a^*_{CDOM}(254)$, were generally low for all sites (0.3 ± 0.3 m^2 g^{-1}, Table S1), implying dominant aliphatic structures of DOM and/or a primary autochthonous source of DOM in the study area.

Table 1
Comparison of DOM properties in this study with previous studies in the Arctic Ocean.

Sampling time and storage	Location	Depth (m)	DOC (mM)	$a_{CDOM}(\lambda)$ (m^{-1})	FDOM[a]	Abundance (RU)	References
Aug. 30-Sep. 5, 2015	Chukchi Shelf	5 to 2240	n/a	3.9 ± 3.4, λ = 254	B	0.35 ± 0.40	In this study
Freezer	Chukchi Basin			1.6 ± 2.2, λ = 350	T	0.24 ± 0.34	
	East Siberian Slope				M	0.04 ± 0.02	
					A	0.07 ± 0.03	
					C	0.03 ± 0.01	
Jul. 17-Oct. 9, 2008	Chukchi Slope	Upper 400	n/a	n/a	A, C	~0.006	Guéguen et al., 2012
Fridge	East Siberian Slope				M	~0.003	
within 6 months					T	~0.006	
					M	~0.01	
					B	~0.02	
Aug. 21-Sep. 27, 2011	Canada Basin	Surface	n/a	0–1.25, λ = 370	M	0–0.08	Guéguen et al., 2015
Fridge	Makarov Basin				A, M, C	0.01–0.07	
within 6 months					A, C	0–0.25	
					M	0.01–0.07	
					B, T	n/a	
Jul.4–17, 2008	Canadian Arctic	4 to 1318	n/a	~0–0.5, λ = 350	A, C	0.01–0.09	Guéguen et al., 2014
Jul.20-Aug.5, 2009	Archipelago;				M	0.005–0.045	
Fridge	Baffin Bay;				Red shifted A, C	0.004–0.022	
within 6 months	Labrador Sea				B, T	0.000–0.035	
Summer, 2005	Canada Basin	2 to 4354	n/a	~0–0.8, λ = 375	n/a		Stedmon et al., 2011
Freezer	Nansen Basin						
Jul. 6, 2011	Chukchi Shelf	Surface or	~0.061	~1.37, λ = 254	Red shifted A, C	0.022	Logvinova et al., 2015
Freezer	Beaufort Sea	Ice-water interface			A, M	0.008	
					T	0.031	
					B	0.032	
					A	0.037	
					A, C	0.010	
Jul. 8–28, 2005	Coastal Canadian	Surface	0.036–0.243	0.14–4.85, λ = 312	A, C	0.003–0.17	Walker et al., 2009
Freezer	Arctic				A	0.003–0.09	
					red shifted A, C	0.001–0.07	
					T	0–0.06	
					B	0.01–0.05	
					M	0.006–0.02	
Sep. 2011	East Siberian Shelf	Surface	n/a	~2–24, λ = 254	n/a	n/a	Pugach et al., 2015

[a] Based on Coble et al. (1998).

The slope ratios (S_R) at site S1 (3.2 ± 0.9) were significantly higher ($p < 0.01$) than those at site S3 (1.9 ± 0.6), implying generally higher CDOM molecular weight at East Siberian Slope site S3 than at Chuckchi Shelf site S1. The FI values at site S4 (1.3 ± 0.1) were significantly lower ($p < 0.001$) than those at sites S1 and S3 (1.9 ± 0.3 and 1.8 ± 0.3, respectively), suggesting terrestrial inputs of fulvic acids to Chukchi Basin site S4. The BIX were relatively high with the values of 1.1 ± 0.3 as opposite to the low levels of HIX (0.8 ± 0.4) for all the samples, further supporting a primary marine/microbial-derived source of DOM.

For FDOM, the intensities of the tyrosine-like peak B at East Siberian Slope site S3 (0.6 ± 0.6 RU) were significant higher than those at Chukchi Shelf site S1 (0.3 ± 0.1 RU, $p < 0.05$) and Chukchi Basin site S4 (0.1 ± 0.1 RU, $p < 0.001$, Table S1). No significant differences were found among the three sites for the other FDOM peaks. However, the average abundances of the protein-like peaks B (0.35 ± 0.40 RU) and T (0.24 ± 0.34 RU) in this study were approximately one order of magnitude higher than those reported in the Arctic Ocean in previous studies (<0.06 RU, Table 1, Walker et al., 2009; Guéguen et al., 2012, 2014; Logvinova et al., 2015). The humic-like moieties, however, were generally low with peaks M, A, and C remaining around 0.04, 0.07, and 0.03 RU, respectively, which were generally comparable to those of the above-mentioned previous reports ranging from ~0.003 to 0.09 RU.

3.3. Vertical distributions of seawater chemistry and DOM parameters

As seen from Fig. 2, both of the absorption coefficients at 254 and 350 nm, along with the aromaticity index $a^*_{CDOM}(254)$, displayed higher values at the surface of Chukchi Basin site S4 or near the bottom, suggesting that a CDOM source from the sediments as well as the riverine input might influence on the surface water of the site S4. Surface waters at all sites and bottom waters at site S4 also displayed higher slope ratio (S_R) values up to ~4, suggesting the presence of smaller molecular sized CDOM for these samples. As for FDOM, the terrestrial humic-like peak C and HIX had similar patterns to the absorption coefficient at 254 and 350 nm, namely $a_{CDOM}(254)$ and $a_{CDOM}(350)$, as well as the aromaticity proxy, specific absorption coefficient $a^*_{CDOM}(254)$, with the higher values near the bottom and at the surface of the site S4 (Fig. 2 and Fig. 3). The protein-like peaks B and T also generally featured higher values in the bottom waters. The salinity versus absorption coefficient $a_{CDOM}(350)$ displayed no significant correlation, potentially due to effects from sea ice melting to the surface waters and sediments inputs to the bottom water samples (Figs. 4a and 4b). The chl-*a* was up to 0.65, 0.90 and 1.52 mg m^{-3} at sites S1, S3, and S4 respectively, and with a monthly average in August 2015 reaching 0.55 to 0.71 mg m^{-3} at site S1 surface waters, which falls in the range of those illustrated in previous fall phytoplankton blooms in this area (~0.5–2.0 mg m^{-3}, Ardyna et al., 2013). It is noteworthy that the chl-*a* below the euphotic zone was still ~0.5 mg m^{-3} through the entire water column. The potential reason for this phenomenon is the unusual months-long phytoplankton bloom in this area from summer to early autumn of 2015 as evidenced by the satellite image (Table 2, Fig. S3), which was observed neither in 2014 nor 2016. Previous reports suggested lateral spreading of water masses and strong wind-driven vertical mixing in this region (Hioki et al., 2014; Uchimiya et al., 2016), which could possibly bring chl-*a* to the entire water column depth.

4. Discussion

4.1. The origins of DOM

The origins of DOM in the Chukchi-East Siberian Seas of the Arctic seawaters are potentially from both autochthonous (i.e., in situ primary

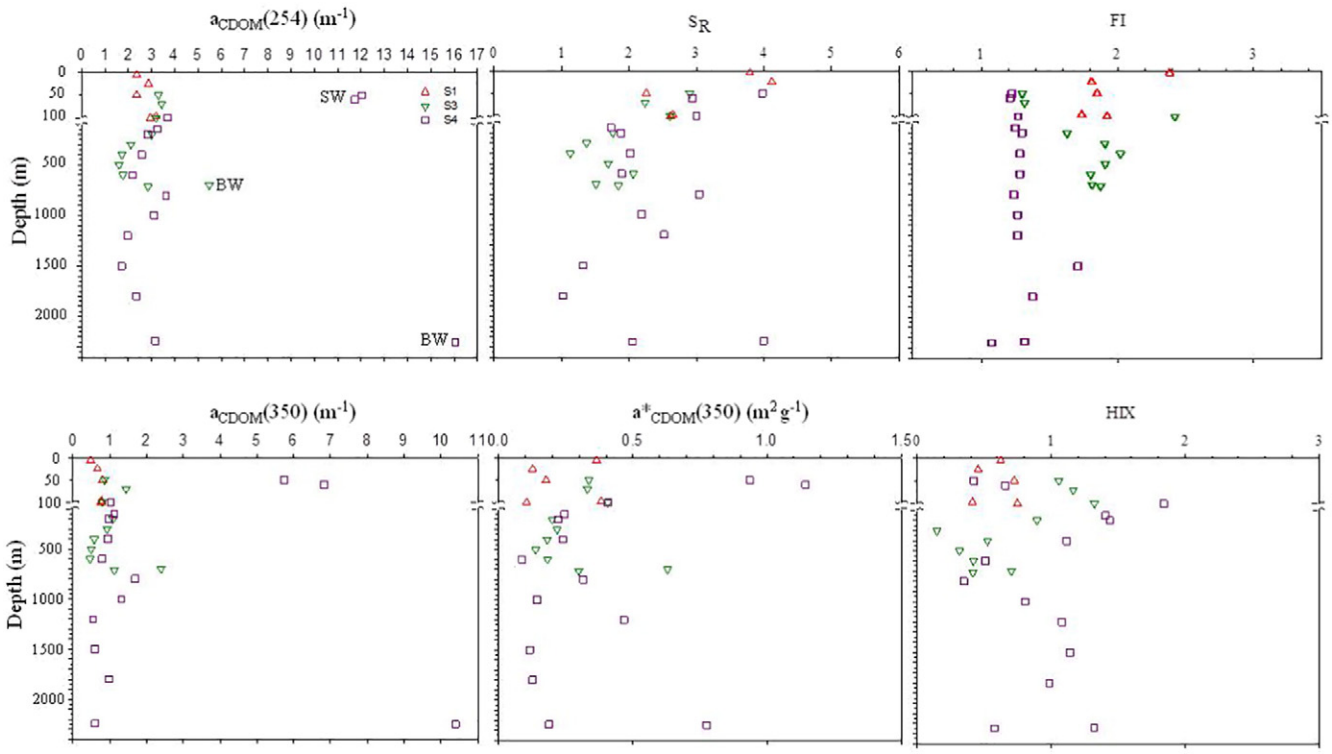

Fig. 2. Vertical profiles of seawater DOM parameters in the Chukchi-East Siberia Sea area. SW = surface water; BW = bottom water.

productivity) and allochothonous (such as riverine runoff, coastal erosion, aeolian inputs, and ice-rafted debris) sources (Stein, 2008). Arctic sediments, especially shelf sediments, can potentially contribute to the FDOM pool by production during early diagenesis from particulate organic matter followed by ensuing benthic efflux (Chen et al., 2016). However, the autochthonous source appears to be dominant for this particular region and the time period considering the relative remoteness of these sites from the influence of large rivers and our supporting data from the low aromaticity index $a^*_{CDOM}(254)$ ($0.3 \pm 0.3\ m^2\ g^{-1}$), high BIX (1.1 ± 0.3), and low HIX (0.8 ± 0.4). Meanwhile, there are hints of potential riverine inputs to the surface waters of Chukchi Basin site S4 as seen from the relatively high CDOM absorption coefficients (~12 and ~6 m^{-1} at 254 and 350 nm, respectively) and relatively low FI (~1.2).

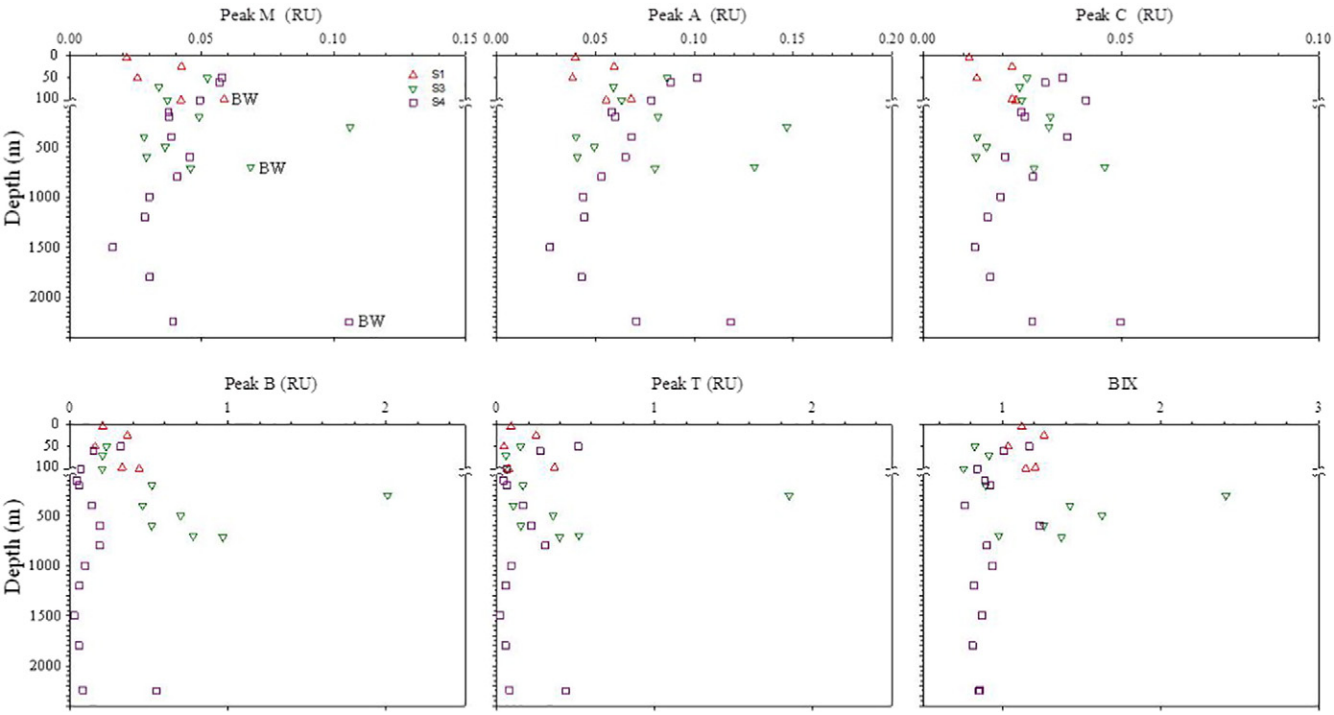

Fig. 3. Vertical profiles of seawater FDOM parameters in the Chukchi-East Siberia Seas of the Arctic Ocean. BW = bottom water.

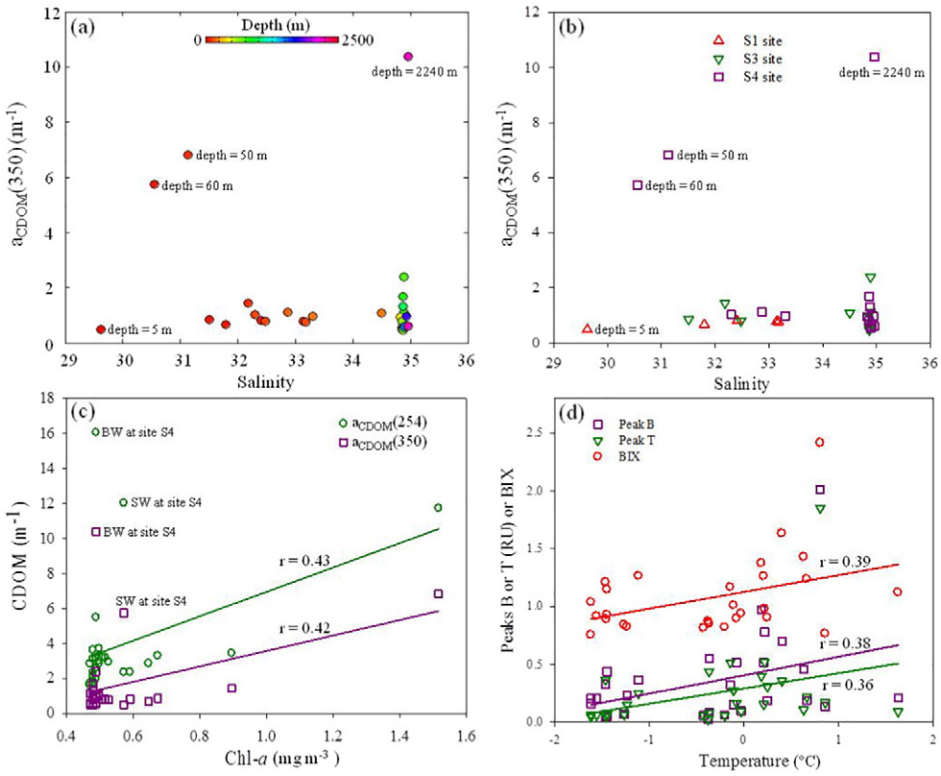

Fig. 4. Relationships among seawater parameters. (a, b) salinity vs. $a_{CDOM}(350)$. (c) Chl-*a* vs. $a_{CDOM}(254)$ and $a_{CDOM}(350)$ ($p < 0.05$). (d)Temperature vs. peaks B and T and BIX ($p < 0.05$). SW = surface water; BW = bottom water.

4.2. High protein-like FDOM caused by fall phytoplankton bloom

The high abundance of protein-like peaks could be linked with a fall phytoplankton bloom in the study area. Dominant protein-like FDOM peaks are considered typical fingerprints for algal-derived DOM (Henderson et al., 2008; Zhang et al., 2013; Chen and Jaffé, 2014). A co-variance between CDOM levels ($a_{CDOM}(254)$ and $a_{CDOM}(350)$) and chl-*a* has also been found in this study ($r = 0.43$ and 0.42, respectively, $p < 0.05$; Fig. 4c), in line with previous reports of CDOM production by marine phytoplankton (Romera-Castillo et al., 2010). Positive correlation between protein-like peaks B and T with BIX has been observed ($r = 0.85$ and 0.79, respectively, $p < 0.0001$; Fig. 5), implying linkage of protein-like FDOM production with biological activity which is consistent with a previous study that found FDOM was produced after the stationary phase by bacteria using non-fluorescent organic matter derived from phytoplankton (Rochelle-Newall and Fisher, 2002). In addition, temperature is positively correlated with protein-like peak B and T and BIX ($r = 0.36$–0.39, $p < 0.05$, Fig. 4d), suggesting the effects of environmental physical condition on the biological activity and consequently the seawater DOM properties. The release of

Table 2
Chlorophyll *a* (chl-*a*) data estimated via in situ fluorescence and remote sensing (monthly average in August 2015).
BW: bottom water. Ave: average value. SD: standard deviation.

Site	Depth (m)	Chl-*a* Fluo[‡] ($mg\,m^{-3}$)	Chl-*a* MODIS-Aqua[a] ($mg\,m^{-3}$)	Chl-*a* MODIS-Terra[a] ($mg\,m^{-3}$)	Site	Depth (m)	Chl-*a* Fluo[‡] ($mg\,m^{-3}$)	Site	Depth (m)	Chl-*a* Fluo[‡] ($mg\,m^{-3}$)
S1	0	–	0.55 (August)	0.71 (August)	S3	50	0.67	S4	50	0.57
	–	–	0.61 (July)	0.66 (July)		–	–	–	–	–
	5	0.57	–	–		70	0.90		60	1.52
	25	0.65	–	–		100	0.52		100	0.50
	50	0.60	–	–		200	0.50		150	0.50
	97	0.51	–	–		300	0.48		200	0.50
(BW)	100	0.53	–	–		400	0.47		400	0.49
	–	–	–	–		500	0.47		600	0.48
	–	–	–	–		600	0.48		800	0.48
	–	–	–	–		700	0.49		1000	0.48
	–	–	–	–	(BW)	715	0.47		1200	0.49
	–	–	–	–		–	–		1500	0.48
	–	–	–	–		–	–		1800	0.48
	–	–	–	–		–	–		2240	0.49
	–	–	–	–		–	–	(BW)	2250	0.49
	Ave:	0.58	–	–		Ave:	0.55		Ave:	0.57
	SD:	0.06	–	–		SD:	0.14		SD:	0.28

Fluo[‡]: estimated from in situ fluorescence data at Ex/Em = 470 nm/695 nm via equation: [Chl-a] = 0.303 × fluorescence + 0.496.
[a] See supporting information for procedures to obtain satellite-derived chl-*a* concentration. BW = bottom water.

protein-like fluorescence due to fresh biomass (including algae) leaching was found to be rapid, and a large amount of FDOM could be released within one day (Chen and Jaffé, 2014). This plausible explanation can also be supported by the sampling time of this study (i.e., a fall season from August 30th to September 5th). Recently, double phytoplankton blooms (both spring and fall) at temperate oceans, triggered by Arctic sea ice loss, were observed by satellite remote sensing of the surface pigments (Ardyna et al., 2014) and also in situ measurement in Chukchi Shelf induced by strong wind followed by vertical mixing (Uchimiya et al., 2016). Perrette et al. (2011) reported near-ubiquity (77–89%) ice-edge blooms in the Arctic, with some long green belts propagating behind the receding ice-edge over hundreds of kilometers and over several months. The sampling sites here are all close to the ice-edge as mentioned above so it is reasonable to catch a fall bloom considering the location and timing.

The chl-*a* data of this study also agree with our explanation. For example, the subsurface maxima appeared at the depths of 25–70 m with the values of 0.65, 0.90, and 1.52 mg m^{-3} at sites S1, S3, and S4, respectively (Fig. 4). Even the average chl-*a* values throughout the entire water column were as high as 0.6 mg m^{-3}, higher than the threshold generally set for algal bloom in these areas (i.e., 0.5 mg m^{-3}, Perrette et al., 2011; Ardyna et al., 2014). Furthermore, surface chl-*a* at ice-free site S1 retrieved from remote sensing agrees well with this, with monthly average in August 2015 reaching up to 0.55 mg m^{-3} (by MODIS-Aqua) and 0.71 mg m^{-3} (by MODIS-Terra) (Table 1, Fig. S2). These chl-*a* levels indicated that the sampling period was in a fall phytoplankton bloom or in an immediate post-bloom season as the previously reported chl-*a* values were ~0.5–2 mg m^{-3} during fall phytoplankton blooms at similar depths in this area (Ardyna et al., 2013). The relative high chl-*a* level below the euphotic zone (~0.5 mg m^{-3}) might be caused by wind-driven vertical mixing and/or detritus shower from the euphotic zone as phytoplankton bloom was observed at Chukchi Shelf site S1 in both July and August of 2015 via remote sensing (Fig. S3).

Although the chl-*a* levels were not extremely high here, it still indicated high phytoplankton biomass as supported by previous chl-*a* and phytoplankton bloom studies. There is great variability of cellular chl-*a* content (e.g., 0.1–9.7% of fresh algal weight) resulting in great variation of ratio of chl-*a* and biomass depending on external and internal factors, including phytoplankton taxonomic composition (major factor), cell physiological conditions, phytoplankton size (inverse relation), light intensity (e.g., "photoacclimation" effect), temperature, and nutrients concentrations (Felip and Catalan, 2000; Boyer et al., 2009; Wang et al., 2009). It is also notable that the relatively low protein-like fluorescence values reported in previous studies were all based on the samples collected in July (Walker et al., 2009; Logvinova et al., 2015). Although the studies of Guéguen et al. (2012, 2014) were based on fall samples, the samples were stored in a refrigerator for up to six months, which might have caused a substantial degradation of the labile pools of DOM such as proteins especially if the samples had not been pre-filtered with sterile filters (0.2 μm). For example, the half-lives of periphyton-derived protein-like DOM (primarily algal source) were known to be as short as hours upon bio-degradation (Chen and Jaffé, 2016). Furthermore, the study area here belongs to the downstream location of nutrient-enriched Pacific water entrained from the Bering Strait through the Chukchi Sea, and/or the upwelling and vertical-mixing area driven by wind or storm along the ice edge (Wang et al., 2005; Ardyna et al., 2014). Taken together, it is highly likely that the fall phytoplankton blooms, promoted by light enrichment and nutrients availability, caused the unusually high abundance of protein-like FDOM in the study area at the time of sampling (fall, 2015). Nevertheless, there is a seemingly discrepancy between the maximum chl-*a* levels and the maximum protein-like fluorescence in that the former was the highest near the surface while the latter was found to be generally higher in subsurface and/or close to the bottom water (Figs. 3 and 6). This could be explained by: (1) potential strong wind-driven vertical mixing as observed previously (Uchimiya et al., 2016), (2) the lateral transport of

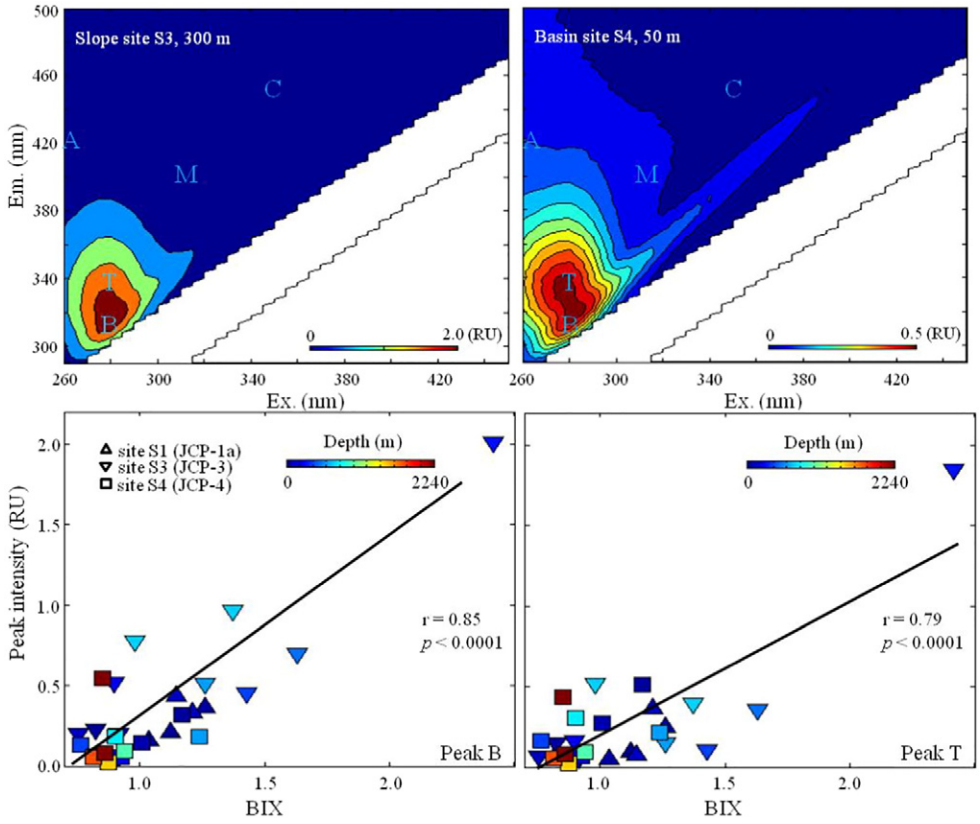

Fig. 5. High abundance of protein-like peaks in EEMs (upper panel) and correlations between the intensity of tyrosine-like (B) and tryptophan-like (T) peaks with biological index (lower panel) suggested phytoplankton bloom in the studying area of the Arctic Ocean from late August to early September 2015.

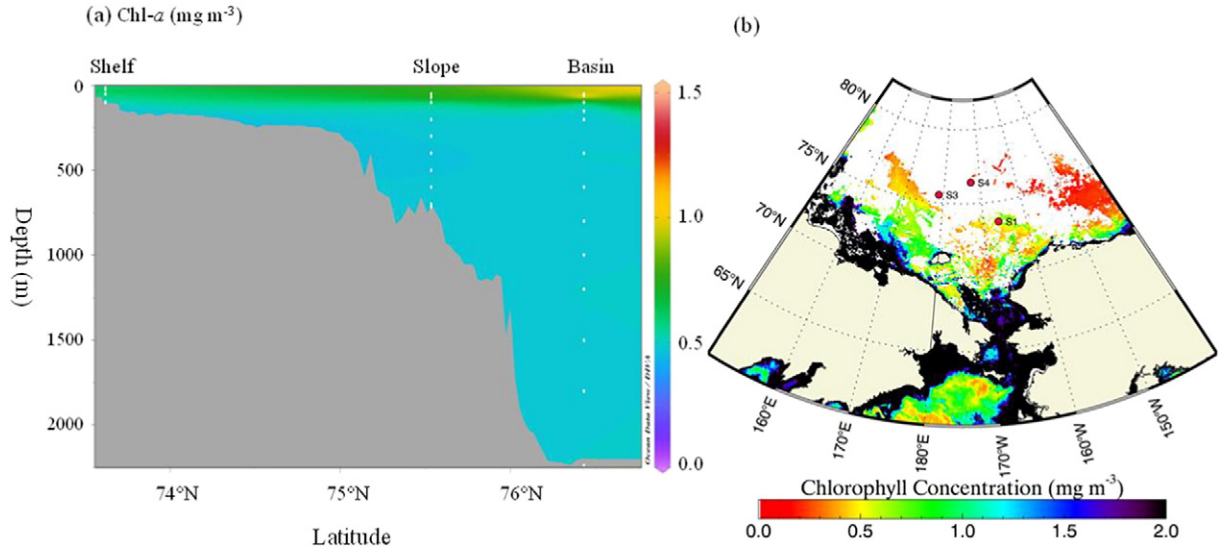

Fig. 6. Vertical sections of seawater chl-*a* concentration along a shelf-slope-basin gradient in the Chukchi-East Siberia Sea (a) and satellite image (MODIS-Aqua) of monthly average chl-*a* concentration in August 2015 in the Arctic (b).

organic materials along a shelf-slope-basin gradient (Hioki et al., 2014), (3) inputs from the marine sediments (Logvinova et al., 2015; Chen et al., 2016), (4) a combination of two or three of the above factors. Although the phytoplankton bloom started at the ocean surface, the detritus could be found in a high amount at the lower depth and sediments following vertical turnover. In addition, the positive correlations between the protein-like peaks B and T with BIX ($R^2 = 0.85$ and 0.79 respectively, $p < 0.0001$; Fig. 5) further supported the microbial/marine-derived source of DOM in this area, in line with findings in a previous report of high bacterial activity and low spectral slopes for CDOM (350 to 500 nm) during summer to fall in the Chuckchi Sea (Matsuoka et al., 2015). A layer of AOU maxima around 200 m and the near exhaustion of nutrient of phosphate (PO_4^{3-}) could be evidence of microbial respiration and remineralization of the sinking particulate organic matter. However, we need to be aware of the inter-annual variations with regard to the timing, intensity, and duration of fall phytoplankton blooms as seen from the satellite image from 2014 to 2016 (Fig. S2–S3).

5. Conclusions and environmental implications

The wide variability of the DOM quantity and quality in the Arctic Ocean indicated the great variations of Arctic DOM dependent on spatial, temporal, and depth (Table 1). Generally high protein-like FDOM (average values 0.1–0.6 RU with maxima values of 2.01 and 1.85 RU for peaks B and T, respectively) were first observed for the seawaters in the Chukchi and East Siberian Seas of the Arctic Ocean from late August to early September 2015. This finding implies the exceptional high occurrence of protein-like DOM because of the general correlations between aromatic amino acids in FDOM and amino acids per se (Yamashita and Tanoue, 2003). Moreover, the intensities of the tyrosine-like peak B and tryptophan-like peak T were positively correlated with biological index, suggesting potential influence of fall phytoplankton blooms on the study area at the time of sampling. This inference is supported by the recent satellite remote sensing observation of double bloom occurrence (spring/summer and fall) triggered by Arctic Ocean sea ice loss as well as the chl-*a* data of this study. Further, it is supported by in situ measurement of fall phytoplankton bloom in Chukchi Shelf which is explained by strong wind-driven vertical mixing (Uchimiya et al., 2016). A subsurface layer (~100–200 m) of AOU maxima also implied the oxidation of the biogenic organic matter sinking from the surface ocean, which are presumably derived from surface primary productivity. CDOM showed maxima levels at the surface of the Chukchi Basin, potentially hinting the riverine influence probably from the Canadian Arctic side rather than from the Siberian Rivers. A positive correlation between CDOM and chl-*a* was observed despite influence from the above-mentioned surface and bottom waters (Fig. 4c). More high-resolution temporal and spatial investigations are warranted to explicitly unveil the variations of DOM characteristics and the ecosystem in the response to the changing environmental forcing. Our results delivers an important message that although double phytoplankton blooms are considered more typical in the temperate oceans, the ongoing climate change may further trigger the regime shift of the ecosystems in the high latitude.

Associated content

Notes: The authors declare no competing financial interest.

Acknowledgements

This work was supported by National Research Foundation of Korea (NRF) grants (No. 2014R1A2A2A09049496 and No. 2015M1A5A1037243) and Research and Development on Geochemical Proxies of Isotope and Trace Element for Understanding of Earth and Universe Evolution Processes (GP2017-018) funded by Korea ministry of Science, ICT, and Future planning. The authors thank the captain and crews of RV Araon for help with sampling during the Arctic expedition in 2015 and Ms. Yun-Kyung Lee for her help with analytical measurements. The authors thank Dr. Mathieu Ardyna for helpful discussion.

Appendix A. Supplementary data

Supplementary data to this article can be found online at http://dx.doi.org/10.1016/j.scitotenv.2017.04.233.

References

Aagaard, K., Carmack, E.C., 1989. The role of sea ice and other fresh water in the Arctic circulation. J. Geophys. Res. Oceans 94 (C10), 14485–14498.
Anderson, L.G., Amon, R.M.W., 2014. In: Hansell, D.A., Carlson, C. (Eds.), Biogeochemistry of Marine Dissolved Organic Matter. Elsevier, pp. 609–630.
Ardyna, M., Babin, M., Gosselin, M., Devred, E., Bélanger, S., Matsuoka, A., Tremblay, J.É., 2013. Parameterization of vertical chlorophyll *a* in the Arctic Ocean: impact of the subsurface chlorophyll maximum on regional, seasonal, and annual primary production estimates. Biogeosciences 10 (6), 4383–4404.
Ardyna, M., Babin, M., Gosselin, M., Devred, E., Rainville, L., Tremblay, J.-É., 2014. Recent Arctic Ocean sea ice loss triggers novel fall phytoplankton blooms. Geophys. Res. Lett. 41 (17), 6207–6212.

Boyer, J.N., Kelble, C.R., Ortner, P.B., Rudnick, D.T., 2009. Phytoplankton bloom status: chlorophyll a biomass as an indicator of water quality condition in the southern estuaries of Florida, USA. Ecol. Indic. 9 (6, Supplement), S56–S67.
Cauwet, G., Sidorov, I., 1996. The biogeochemistry of Lena River: organic carbon and nutrients distribution. Mar. Chem. 53 (3–4), 211–227.
Chen, M., Jaffé, R., 2014. Photo- and bio-reactivity patterns of dissolved organic matter from biomass and soil leachates and surface waters in a subtropical wetland. Water Res. 61 (0), 181–190.
Chen, M., Jaffé, R., 2016. Quantitative assessment of photo- and bio-reactivity of chromophoric and fluorescent dissolved organic matter from biomass and soil leachates and from surface waters in a subtropical wetland. Biogeochemistry:1–17 http://dx.doi.org/10.1007/s10533-016-0231-7.
Chen, M.L., Price, R.M., Yamashita, Y., Jaffé, R., 2010. Comparative study of dissolved organic matter from groundwater and surface water in the Florida coastal Everglades using multi-dimensional spectrofluorometry combined with multivariate statistics. Appl. Geochem. 25 (6), 872–880.
Chen, M., Kim, J.-H., Nam, S.-I., Niessen, F., Hong, W.-L., Kang, M.-H., Hur, J., 2016. Production of fluorescent dissolved organic matter in Arctic Ocean sediments. Sci. Rep. 6, 39213.
Coble, P.G., Del Castillo, C.E., Avril, B., 1998. Distribution and optical properties of CDOM in the Arabian Sea during the 1995 Southwest Monsoon. Deep-Sea Res. II Top. Stud. Oceanogr. 45 (10—11), 2195–2223.
Comiso, J.C., 2002. A rapidly declining perennial sea ice cover in the Arctic. Geophys. Res. Lett. 29 (20) (17-11-17-14).
Cory, R.M., Ward, C.P., Crump, B.C., Kling, G.W., 2014. Sunlight controls water column processing of carbon in arctic fresh waters. Science 345 (6199), 925–928.
Cullen, J.J., 1982. The deep chlorophyll maximum: comparing vertical profiles of chlorophyll a. Can. J. Fish. Aquat. Sci. 39 (5), 791–803.
Felip, M., Catalan, J., 2000. The relationship between phytoplankton biovolume and chlorophyll in a deep oligotrophic lake: decoupling in their spatial and temporal maxima. J. Plankton Res. 22 (1), 91–106.
Gieskes, J.M., Gamo, T., Brumsack, H., 1991. Chemical Methods for Interstitial Water Analysis Aboard JOIDES Resolution. pp. 1–60.
Grebmeier, J.M., McRoy, C.P., Feder, H.M., 1988. Pelagic-benthic coupling on the shelf of the northern Bering and Chukchi Seas. I. Food supply source and benthic biomass. Mar. Ecol. Prog. Ser. 48, 57–67.
Guéguen, C., McLaughlin, F.A., Carmack, E.C., Itoh, M., Narita, H., Nishino, S., 2012. The nature of colored dissolved organic matter in the southern Canada Basin and East Siberian Sea. Deep-Sea Res. II Top. Stud. Oceanogr. 81–84, 102–113.
Guéguen, C., Cuss, C.W., Cassels, C.J., Carmack, E.C., 2014. Absorption and fluorescence of dissolved organic matter in the waters of the Canadian Arctic Archipelago, Baffin Bay, and the Labrador Sea. J. Geophys. Res. Oceans 119 (3), 2034–2047.
Guéguen, C., Itoh, M., Kikuchi, T., Eert, J., Williams, W.J., 2015. Variability in dissolved organic matter optical properties in surface waters in the Amerasian Basin. Front. Mar. Sci. 2.
Helms, J.R., Stubbins, A., Ritchie, J.D., Minor, E.C., Kieber, D.J., Mopper, K., 2008. Absorption spectral slopes and slope ratios as indicators of molecular weight, source, and photobleaching of chromophoric dissolved organic matter. Limnol. Oceanogr. 53 (3), 955–969.
Henderson, R.K., Baker, A., Parsons, S.A., Jefferson, B., 2008. Characterisation of algogenic organic matter extracted from cyanobacteria, green algae and diatoms. Water Res. 42 (13), 3435–3445.
Hioki, N., Kuma, K., Morita, Y., Sasayama, R., Ooki, A., Kondo, Y., Obata, H., Nishioka, J., Yamashita, Y., Nishino, S., Kikuchi, T., Aoyama, M., 2014. Laterally spreading iron, humic-like dissolved organic matter and nutrients in cold, dense subsurface water of the Arctic Ocean. Sci. Rep. 4. http://dx.doi.org/10.1038/srep06775.
Holmes, R.M., McClelland, J.W., Peterson, B.J., Tank, S.E., Bulygina, E., Eglinton, T.I., Gordeev, V.V., Gurtovaya, T.Y., Raymond, P.A., Repeta, D.J., Staples, R., Striegl, R.G., Zhulidov, A.V., Zimov, S.A., 2012. Seasonal and annual fluxes of nutrients and organic matter from large rivers to the Arctic Ocean and surrounding seas. Estuar. Coasts 35 (2), 369–382.
Hugelius, G., Strauss, J., Zubrzycki, S., Harden, J.W., Schuur, E.A.G., Ping, C.L., Schirrmeister, L., Grosse, G., Michaelson, G.J., Koven, C.D., O'Donnell, J.A., Elberling, B., Mishra, U., Camill, P., Yu, Z., Palmtag, J., Kuhry, P., 2014. Estimated stocks of circumpolar permafrost carbon with quantified uncertainty ranges and identified data gaps. Biogeosciences 11 (23), 6573–6593.
Huguet, A., Vacher, L., Relexans, S., Saubusse, S., Froidefond, J.M., Parlanti, E., 2009. Properties of fluorescent dissolved organic matter in the Gironde Estuary. Org. Geochem. 40 (6), 706–719.
Hur, J., Cho, J., 2012. Prediction of BOD, COD, and total nitrogen concentrations in a typical Urban River using a fluorescence excitation-emission matrix with PARAFAC and UV absorption indices. Sensors 12, 972–986.
Inoue, J., Yamazaki, A., Ono, J., Dethloff, K., Maturilli, M., Neuber, R., Edwards, P., Yamaguchi, H., 2015. Additional Arctic observations improve weather and sea-ice forecasts for the Northern Sea Route. Sci. Rep. 5, 16868.
KIGAM, 2015. Preliminary survey for marine energy resources in the Arctic region. Daejeon. p. 141.
Kim, J.-H., Torres, M.E., Hong, W.-L., Choi, J., Riedel, M., Bahk, J.-J., Kim, S.-H., 2013. Pore fluid chemistry from the second gas hydrate drilling expedition in the Ulleung Basin (UBGH2): source, mechanisms and consequences of fluid freshening in the central part of the Ulleung Basin, East Sea. Mar. Pet. Geol. 47, 99–112.
Lawaetz, A.J., Stedmon, C.A., 2009. Fluorescence intensity calibration using the Raman scatter peak of water. Appl. Spectrosc. 63 (8), 936–940.
Liu, J., Curry, J.A., Hu, Y., 2004. Recent Arctic Sea ice variability: connections to the Arctic oscillation and the ENSO. Geophys. Res. Lett. 31 (9), L09211. http://dx.doi.org/10.01029/02004GL019858.
Logvinova, C.L., Frey, K.E., Mann, P.J., Stubbins, A., Spencer, R.G.M., 2015. Assessing the potential impacts of declining Arctic sea ice cover on the photochemical degradation of dissolved organic matter in the Chukchi and Beaufort Seas. J. Geophys. Res. Biogeosci. 120 (11), 2326–2344.
Mann, P.J., Spencer, R.G., Hernes, P.J., Six, J., Aiken, G.R., Tank, S.E., McClelland, J.W., Butler, K.D., Dyda, R.Y., Holmes, R.M., 2016. Pan-arctic trends in terrestrial dissolved organic matter from optical measurements. Front. Earth Sci.:4 http://dx.doi.org/10.3389/feart.2016.00025.
Matsuoka, A., Ortega-Retuerta, E., Bricaud, A., Arrigo, K.R., Babin, M., 2015. Characteristics of colored dissolved organic matter (CDOM) in the Western Arctic Ocean: relationships with microbial activities. Deep-Sea Res. II Top. Stud. Oceanogr. 118, 44–52.
McKnight, D.M., Boyer, E.W., Westerhoff, P.K., Doran, P.T., Kulbe, T., Andersen, D.T., 2001. Spectrofluorometric characterization of dissolved organic matter for indication of precursor organic material and aromaticity. Limnol. Oceanogr. 46 (1), 38–48.
Morison, J., Kwok, R., Peralta-Ferriz, C., Alkire, M., Rigor, I., Andersen, R., Steele, M., 2012. Changing Arctic Ocean freshwater pathways. Nature 481 (7379), 66–70.
Nishino, S., Kawaguchi, Y., Inoue, J., Hirawake, T., Fujiwara, A., Futsuki, R., Onodera, J., Aoyama, M., 2015. Nutrient supply and biological response to wind-induced mixing, inertial motion, internal waves, and currents in the northern Chukchi Sea. J. Geophys. Res. Oceans 120 (3), 1975–1992.
Parlanti, E., Wörz, K., Geoffroy, L., Lamotte, M., 2000. Dissolved organic matter fluorescence spectroscopy as a tool to estimate biological activity in a coastal zone submitted to anthropogenic inputs. Org. Geochem. 31 (12), 1765–1781.
Perrette, M., Yool, A., Quartly, G.D., Popova, E.E., 2011. Near-ubiquity of ice-edge blooms in the Arctic. Biogeosciences 8 (2), 515–524.
Pugach, S.P., Pipko, I.I., Semiletov, I.P., Sergienko, V.I., 2015. Optical characteristics of the colored dissolved organic matter on the East Siberian shelf. Dokl. Earth Sci. 465 (2), 1293–1296.
Rachold, V., Eicken, H., Gordeev, V.V., Grigoriev, M.N., Hubberten, H.-W., Lisitzin, A.P., Shevchenko, V.P., Schirrmeister, L., 2004. In: Stein, R., MacDonald, R.W. (Eds.), The Organic Carbon Cycle in the Arctic Ocean. Springer Berlin Heidelberg, Berlin, Heidelberg, pp. 33–55.
Raymond, P.A., McClelland, J.W., Holmes, R.M., Zhulidov, A.V., Mull, K., Peterson, B.J., Striegl, R.G., Aiken, G.R., Gurtovaya, T.Y., 2007. Flux and age of dissolved organic carbon exported to the Arctic Ocean: a carbon isotopic study of the five largest arctic rivers. Glob. Biogeochem. Cycles 21 (4). http://dx.doi.org/10.1029/2007GB002934.
Rochelle-Newall, E.J., Fisher, T.R., 2002. Production of chromophoric dissolved organic matter fluorescence in marine and estuarine environments: an investigation into the role of phytoplankton. Mar. Chem. 77 (1), 7–21.
Romera-Castillo, C., Sarmento, H., Alvarez-Salgado, X.A., Gasol, J.M., Marrase, C., 2010. Production of chromophoric dissolved organic matter by marine phytoplankton. Limnol. Oceanogr. 55 (1), 446–454.
Sakshaug, E., 2004. In: Stein, R., Macdonald, R.W. (Eds.), The Organic Carbon Cycle in the Arctic Ocean. Springer-Verlag, Heidelberg, pp. 57–82.
Schlitzer, R., 2016. Ocean Data View. (version 4.7.6). http://odv.awi.de.
Spencer, R.G.M., Aiken, G.R., Butler, K.D., Dornblaser, M.M., Striegl, R.G., Hernes, P.J., 2009. Utilizing chromophoric dissolved organic matter measurements to derive export and reactivity of dissolved organic carbon exported to the Arctic Ocean: a case study of the Yukon River, Alaska. Geophys. Res. Lett. 36.
Stedmon, C.A., Markager, S., 2001. The optics of chromophoric dissolved organic matter (CDOM) in the Greenland Sea: an algorithm for differentiation between marine and terrestrially derived organic matter. Limnol. Oceanogr. 46 (8), 2087–2093.
Stedmon, C.A., Amon, R.M.W., Rinehart, A.J., Walker, S.A., 2011. The supply and characteristics of colored dissolved organic matter (CDOM) in the Arctic Ocean: Pan Arctic trends and differences. Mar. Chem. 124 (1–4), 108–118.
Stein, R., 2008. In: Chamley, H. (Ed.), Developments in Marine Geology. Elsevier.
Thieme, L., Graeber, D., Kaupenjohann, M., Siemens, J., 2016. Fast-freezing with liquid nitrogen preserves bulk dissolved organic matter concentrations, but not its composition. Biogeosciences 13 (16), 4697–4705.
Thompson, D.W.J., Wallace, J.M., 1998. The Arctic oscillation signature in the wintertime geopotential height and temperature fields. Geophys. Res. Lett. 25 (9), 1297–1300.
Uchimiya, M., Motegi, C., Nishino, S., Kawaguchi, Y., Inoue, J., Ogawa, H., Nagata, T., 2016. Coupled response of bacterial production to a wind-induced fall phytoplankton bloom and sediment resuspension in the Chukchi Sea Shelf, Western Arctic Ocean. Front. Mar. Sci. 3 (231).
Walker, S.A., Amon, R.M.W., Stedmon, C., Duan, S.W., Louchouarn, P., 2009. The use of PARAFAC modeling to trace terrestrial dissolved organic matter and fingerprint water masses in coastal Canadian Arctic surface waters. J. Geophys. Res. Biogeosci. 114.
Walker, S.A., Amon, R.M.W., Stedmon, C.A., 2013. Variations in high-latitude riverine fluorescent dissolved organic matter: a comparison of large Arctic rivers. J. Geophys. Res. Biogeosci. 118 (4), 1689–1702.
Wang, J., Cota, G.F., Comiso, J.C., 2005. Phytoplankton in the Beaufort and Chukchi Seas: distribution, dynamics, and environmental forcing. Deep-Sea Res. II Top. Stud. Oceanogr. 52 (24–26), 3355–3368.
Wang, X.J., Behrenfeld, M., Le Borgne, R., Murtugudde, R., Boss, E., 2009. Regulation of phytoplankton carbon to chlorophyll ratio by light, nutrients and temperature in the Equatorial Pacific Ocean: a basin-scale model. Biogeosciences 6 (3), 391–404.
Weishaar, J.L., Aiken, G.R., Bergamaschi, B.A., Fram, M.S., Fujii, R., Mopper, K., 2003. Evaluation of specific ultraviolet absorbance as an indicator of the chemical composition and reactivity of dissolved organic carbon. Environ. Sci. Technol. 37 (20), 4702–4708.
Yamashita, Y., Tanoue, E., 2003. Chemical characterization of protein-like fluorophores in DOM in relation to aromatic amino acids. Mar. Chem. 82 (3–4), 255–271.
Zhang, Y.L., Liu, X.H., Wang, M.Z., Qin, B.Q., 2013. Compositional differences of chromophoric dissolved organic matter derived from phytoplankton and macrophytes. Org. Geochem. 55, 26–37.
Zsolnay, A., Baigar, E., Jimenez, M., Steinweg, B., Saccomandi, F., 1999. Differentiating with fluorescence spectroscopy the sources of dissolved organic matter in soils subjected to drying. Chemosphere 38 (1), 45–50.